Superlattice formation lifting degeneracy protected by nonsymmorphic symmetry through a metal-insulator transition in RuAs

Hisashi Kotegawa,[1] Keiki Takeda,[2] Yoshiki Kuwata,[1] Junichi Hayashi,[2] Hideki Tou,[1] Hitoshi Sugawara,[1] Takahiro Sakurai,[3] Hitoshi Ohta,[1,4] and Hisatomo Harima[1]

[1]*Department of Physics, Kobe University, Kobe 658-8530, Japan*

[2]*Muroran Institute of Technology, Muroran, Hokkaido 050-8585, Japan*

[3]*Research Facility Center for Science and Technology, Kobe University, Kobe, Hyogo 657-8501, Japan*

[4]*Molecular Photoscience Research Center, Kobe University, Kobe, Hyogo 657-8501, Japan*

(Received 18 December 2017; revised manuscript received 14 March 2018; published 4 May 2018)

A single crystal of RuAs obtained with the Bi-flux method shows obvious successive metal-insulator transitions at $T_{MI1} \sim 255$ K and $T_{MI2} \sim 195$ K. The x-ray diffraction measurement reveals the formation of a superlattice of $3\times3\times3$ of the original unit cell below T_{MI2}, accompanied by a change of the crystal system from the orthorhombic structure to the monoclinic one. Simple dimerization of the Ru ions is not seen in the ground state. The multiple As sites observed in the nuclear quadrupole resonance spectrum also demonstrate the formation of the superlattice in the ground state, which is clarified to be nonmagnetic. The divergence in $1/T_1$ at T_{MI1} shows that a symmetry lowering by the metal-insulator transition is accompanied by strong critical fluctuations of some degrees of freedom. Using the structural parameters in the insulating state, the first-principles calculation reproduces successfully the reasonable size of nuclear quadrupole frequencies ν_Q for the multiple As sites, ensuring the high validity of the structural parameters. The calculation also gives a remarkable suppression in the density of states near the Fermi level, although the gap opening is insufficient. A coupled modulation of the calculated Ru d-electron numbers and the crystal structure proposes the formation of a charge density wave in RuAs. Some lacking factors remain, but it is shown that a lifting of degeneracy protected by the nonsymmorphic symmetry through the superlattice formation is a key ingredient for the metal-insulator transition in RuAs.

DOI: 10.1103/PhysRevMaterials.2.055001

I. INTRODUCTION

The metal-insulator transition derived by a drastic revolution in conductivity is an exotic phenomenon in condensed matter physics. Except for a gap opening induced by strong electronic correlations, it is generally a cooperative symmetry breaking brought by a coupling of the Fermi surface instability and degrees of freedom in a solid, such as charge, spin, orbitals, or multipoles [1–5]. Symmetry of crystal is a key ingredient to understand a picture of the metal-insulator transition. If material is low-dimensional, typically composed of a one-dimensional linear chain, it generally possesses a Fermi surface with a good nesting. It promotes a Peierls transition, opening a gap at the Fermi level [1]. In the case in which spins contribute to the Peierls transition, it is often characterized by a dimerization to produce a spin singlet [2]. If material is highly symmetric, on the other hand, the ions can be located under high local symmetry, inducing the orbital degeneracy or multipole degeneracy. A contribution of such degrees of freedom to a metal-insulator transition is a debated topic [3–5].

In 2012 Hirai *et al.* reported that simple binary RuP and RuAs undergo a metal-insulator transition [6]. RuP and RuAs crystallize in the orthorhombic structure in the space group of $Pnma$. The nearest-neighbor Ru ions form a zigzag chain along the a axis, while the second- and third-nearest-neighbor Ru ions form a zigzag ladder along the b axis. This structure is neither a simple low-dimensional one nor a high-symmetric one. Two successive metal-insulator transitions have been reported in the polycrystalline samples [6], and this behavior is more remarkable in RuP than in RuAs, and it disappears in the isostructural RuSb. For RuAs, the transition temperatures have been estimated to be 250 K and 190 K, which are denoted as T_{MI1} and T_{MI2} in this paper. Interestingly, a Rh doping to RuAs and RuP strongly suppresses the insulating state, and induces superconductivity [6,7]. An intriguing question is what triggers the metal-insulator transition of these materials. The previous band calculation has suggested that the topology of the Fermi surface is similar between RuAs and RuP, and that of RuSb differs from two compounds [8]. RuAs and RuP possess degenerate flat bands near the Fermi level, which originate mainly from the $4d_{xy}$ orbitals of Ru; therefore, it is expected that the splitting of the flat band is related to the metal-insulator transition. A charge density wave (CDW) may be realized, but the nesting property of the Fermi surface is not so clear, because these are not simple low-dimensional materials. Photoemission measurement has not detected a typical feature of a CDW transition for the polycrystalline RuP [9]; that is, the charge distribution of the Ru orbital is not clearly seen. Except for the CDW scenario, the contribution of pseudodegeneracy of the d orbitals and the possibility of a spin-singlet formation have been discussed [7,9], but the mechanism of the metal-insulator transition is still undetermined.

Recently, physical properties of a single crystal of RuP made with the Sn-flux method have been reported [10,11]. The crystal shows clear successive transitions at 320 K and 270 K,

but the ground state of the single crystal is metallic in contrast to the polycrystalline sample. The structural transition originating from the formation of a superlattice has been confirmed at room temperature for single-crystal RuP [6,10], whereas the structure of the polycrystalline sample at room temperature is still in the original *Pnma* [6,12]. The formation of a superlattice is a key feature to reveal the origin of the metal-insulator transition of these materials, but unfortunately inconsistency of the physical properties of RuP between single crystals and polycrystals complicates the problem. In this paper, we focus on RuAs to investigate the origin of the metal-insulator transition. A single crystal of RuAs, whose properties are similar to the polycrystalline ones, was successfully obtained using the Bi-flux method.

II. EXPERIMENTAL PROCEDURE

To make the single crystal, the starting materials of Ru : As : Bi = 1 : 1 : 35 were sealed in a silica tube, and they were heated up to 1050 °C, followed by a slow cooling with a rate of −5 °C/h down to 600 °C. After centrifugation, small single crystals with a maximum long axis of about 0.5 mm were obtained. The crystals made by this procedure are denoted as No. 1. Another procedure was attempted as No. 2; the starting composition of Ru : As : Bi = 1 : 1 : 25, the maximum temperature of 1100 °C, and the cooling rate of −3 °C/h. The size of crystals was similar between No. 1 and No. 2, but the sequence for No. 2 was effective to reduce the by-product $RuAs_2$. We also tried the Sn-flux method, but it failed to yield single crystals of RuAs. Very small single crystals of RuP are also obtained using the Bi-flux method, but the resistivity does not show insulating behavior, and the overall behavior resembles that of the single crystal made with the Sn-flux method [10].

The electrical resistivity (ρ) of RuAs was measured using a four-probe method, in which electrical contacts of wire were made by a spot-weld method. The current direction could not be confirmed owing to the smallness of the crystal, but it is expected to be perpendicular to the a axis on the analogy of the Laue experiment for other crystals. The high pressure was applied by utilizing an indenter-type pressure cell and Daphne 7474 as a pressure-transmitting medium [13,14]. Magnetic susceptibility measurement was performed by utilizing a magnetic property measurement system (MPMS; Quantum Design). X-ray diffraction measurements using a single crystal were made on a Rigaku Saturn 724 diffractometer using multilayer mirror monochromated Mo-Kα radiation. A small single crystal of $0.04\times0.04\times0.03$ mm^3 was used for the measurement. The data were collected to a maximum 2θ value of ∼62° using the angle scans. For all structure analyses, the program suite SHELX was used for structure solution and least-squares refinement [15]. PLATON was used to check for missing symmetry elements in the structures [16]. We also performed nuclear quadrupole resonance (NQR) and nuclear magnetic resonance (NMR) for RuAs using a ^{75}As nucleus with a nuclear spin of $I = 3/2$. Band calculations were obtained through a full-potential LAPW (linear augmented plane wave) calculation within the LDA (local density approximation).

III. RESULTS AND DISCUSSION

A. Resistivity, pressure effect, and magnetization

Figure 1(a) shows the temperature dependence of ρ for a single crystal of RuAs. The ρ is almost constant at high temperatures down to $T_{MI1} = 250$ K, and possesses a clear kink at T_{MI1}, below which ρ starts to increase. A sharp transition appears at $T_{MI2} = 190$ K, followed by a clear insulating behavior down to the lowest temperature. As shown in the inset, the transition at T_{MI2} possesses obvious hysteresis similarly to the polycrystalline sample [6], while hysteresis was not visible at T_{MI1}. The increase in ρ below T_{MI2} is much larger than that of the polycrystalline sample, indicating that a contribution from possible conductive impurities can be avoided in the measurement using the single crystal. A fitting of the resistivity data into a typical activation form of $\rho(T) \propto \exp(E_g/2k_BT)$ between 50 K and $T_{MI2} = 190$ K gives the energy gap of $E_g = 340$ K. ρ deviates from the simple activation form below 50 K.

Figure 1(b) shows the pressure variation of ρ for RuAs up to 3.34 GPa. Both T_{MI1} and T_{MI2} increase slightly with increasing pressure. The rates were estimated to be +3.6 K/GPa for T_{MI1} and +0.8 K/GPa for T_{MI2}, respectively. This tendency suggests that the stronger hybridization induced by a smaller volume stabilizes the insulating state, consistent with RuP being more insulating.

Figure 2 shows the temperature dependence of the magnetic susceptibility measured at 1 T on the cooling process. The overall behavior is similar to that obtained in the polycrystalline sample [6], but the transitions become much sharper. The kink at $T_{MI1} = 255$ K is continuous, while the discrete drop was observed at $T_{MI2} = 200$ K. The ground state is dominated by diamagnetism as well as the polycrystalline sample [6]. In the metallic state, the susceptibility is temperature-independent; that is, Curie-Weiss-like behavior is absent. Here, we used the single crystal No. 2, and both T_{MI1} and T_{MI2} are slightly higher

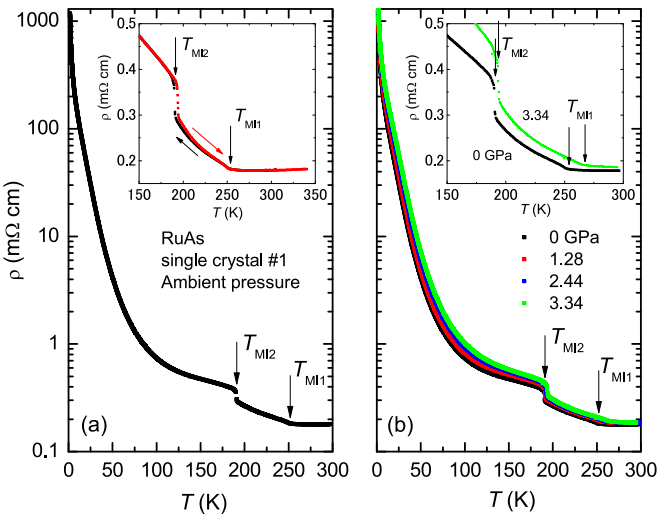

FIG. 1. (a) Temperature dependence of ρ for RuAs at ambient pressure. The resistivity shows clearly two successive metal-insulator transitions at T_{MI1} and T_{MI2}. The inset shows the hysteresis behavior at T_{MI2}. (b) The pressure dependence of ρ for RuAs. Both transition temperatures increase with elevating pressure up to 3.34 GPa.

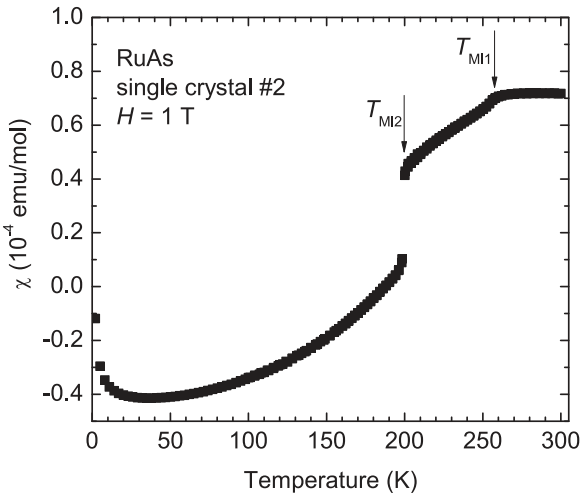

FIG. 2. Temperature dependence of the magnetic susceptibility measured for many pieces of single crystals at 1 T. Two successive transitions can be seen clearly. The T_{MI1} and T_{MI2} for No. 2 are slightly higher than those of No. 1.

than those of No. 1 determined in Fig. 1. We confirmed that there is small sample dependence among the procedures in the sample preparation. It is speculated that they originate from the amount of deficiency of As, as described below.

B. Structural analysis by x-ray diffraction measurement

Next, we performed a structural analysis of RuAs using a single crystal No. 2. Figure 3 shows single-crystal x-ray diffraction patterns at (a) 293 K > T_{MI1} and (b) 170 K < T_{MI2}. The crystal system above T_{MI1} was confirmed to be orthorhombic as reported previously [6,17]. In the insulating state below T_{MI2}, the superlattice spots are clearly observed. They appear at the positions of 0 $k/3$ $l/3$ for the 0kl plane and $h/3$ 0 $l/3$ for the $h0l$ plane, while they are visible only at the positions of $h + 1/3$ $k + 2/3$ 0 or $h + 2/3$ $k + 1/3$ 0 for the $hk0$ plane. As shown by the blue line, a new periodicity can be regarded as 3×3×3, but the asymmetric arrangement of the superlattice spots for the $hk0$ plane reveals that the unit cell below T_{MI2} is not orthorhombic but monoclinic; therefore, the size of the unit cell is smaller than that of the 3×3×3 cell. In the intermediate phase between T_{MI1} and T_{MI2}, on the other hand, the superlattice spots also appear (not shown) and are likely to be incommensurate, but a detailed structural analysis has not been performed successfully yet. Tables I and II show the crystallographic data and the structural parameters for the respective sites at 293 K and 170 K obtained by the present experiments and analyses described in the section on the experimental procedure. In the metallic state above T_{MI1}, the space group of $Pnma$ and the lattice parameters are consistent with the previous reports for the polycrystalline samples [6,17]. As shown in Table II, the analysis suggests that a small amount of deficiency of As is present (∼1%). We consider that the degree of the deficiency induces the sample dependence of the transition temperatures in RuAs, but it is not as serious as it changes the ground state drastically.

The resultant crystal structures are shown in Fig. 4. The structure in $Pnma$ contains the equivalent 4 Ru and 4 As

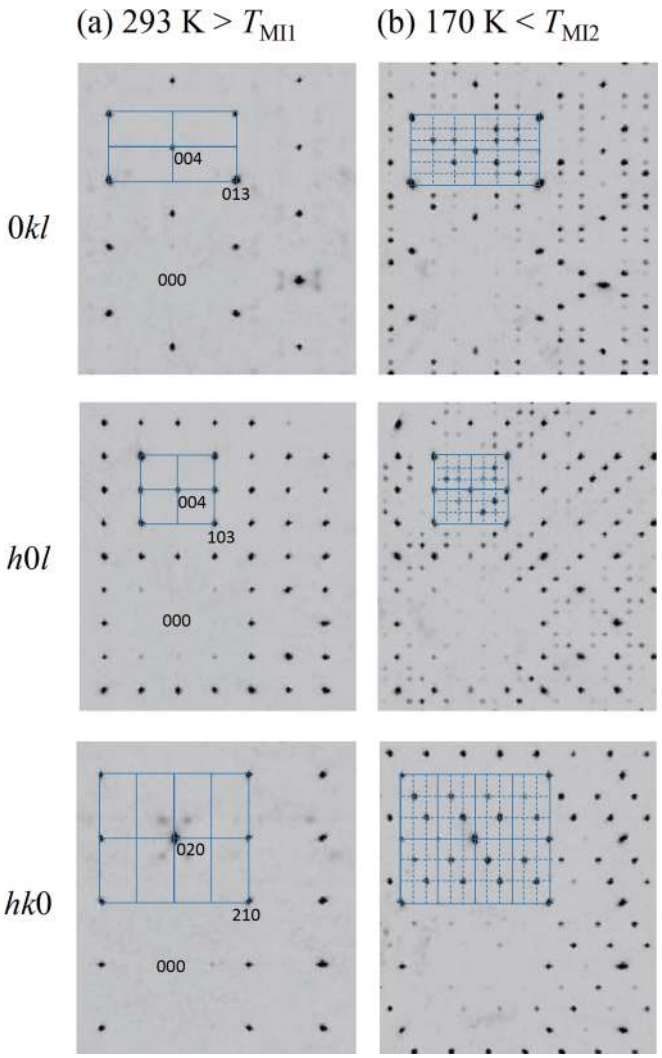

FIG. 3. Single-crystal x-ray diffraction patterns for RuAs at (a) 293 K and (b) 170 K. Reciprocal lattice vectors are shown for the orthorhombic $Pnma$ symmetry. The superlattice spots are seen below T_{MI2}. The new periodicity can be regarded as 3×3×3, but the unit cell is found to be monoclinic from the superlattice spots in the $hk0$ plane.

atoms in the unit cell, as shown in Fig. 4(a). In the ground state below T_{MI2}, the system transforms to the monoclinic structure in $P2_1/c$, in which the inequivalent 9 Ru and 9 As sites exist, and totally 36 Ru and 36 As atoms are included in the unit cell. Therefore, the unit cell in the insulating state is comparable to 9 unit cells of the original structure in $Pnma$. The c axis in $Pnma$ just corresponds to the b axis in $P2_1/c$, whose length is 3 times as long as the original lattice constant. As shown in the figure, the ab plane in $Pnma$ corresponds to the ac plane in $P2_1/c$. The blue line in Fig. 4(d) indicates the unit cell of the monoclinic structure, while the red line indicates the 3×3 cell of the original unit cell. The new threefold periodicity can be confirmed for each direction.

Figure 4(e) shows the zigzag chains of the Ru ions at low temperatures. In $Pnma$, the Ru ions form the perfect zigzag chain consisting of the equivalent sites along the a axis, while it slightly deforms in $P2_1/c$. Chain 1 is composed of an

TABLE I. Crystallographic data of RuAs for the metallic and insulating phases.

Temperature	293 K	170 K
Formula	RuAs	Ru_9As_9
Crystal system	orthorhombic	monoclinic
Space group	*Pnma* (No. 62)	$P2_1/c$ (No. 14)
a (Å)	5.724(3)	6.624(3)
b (Å)	3.3283(14)	18.974(7)
c (Å)	6.323(3)	8.759(4)
β (°)	90	100.843(6)
V (Å^3)	120.46(10)	1082.8(8)
Z	4	4
Unique reflections	212	3279
Residual factor $R1$	0.0402	0.0354
$wR2$	0.0914	0.0785

alternation of 6 different Ru sites, while chain 2 includes an alternation of 3 sites. The respective distances between the neighboring Ru ions are shown, but they are featureless and do not show a clear indication of a dimerization of the Ru ions. Absence of dimerization is obviously supported by an odd number of Ru sites in the unit cell, excluding the possibility of a spin-singlet formation in the insulating state. As shown in Fig. 4(f), on the other hand, the clear threefold periodicity of the bond length can be seen along the original b axis, where the bonding built a linear chain with equal intervals of 3.328 Å in the metallic phase. In a linear chain, for example, the Ru1-Ru6 and Ru3-Ru6 bondings shrink to ∼3.1 Å, while the Ru1-Ru3 bonding significantly extends to ∼3.66 Å. This tendency is commonly seen for all the bondings along the original b axis. This key feature in the deformed structure will be discussed in the final part, together with results of a band calculation.

C. Nuclear quadrupole/magnetic resonance

We performed NMR/NQR measurements to investigate the microscopic state of RuAs. Figures 5(a) and 5(b) show the NMR spectrum measured at around 8 T and the NQR spectrum measured at zero field, respectively. We used many pieces of small single crystals for both measurements; therefore, the experimental condition is similar to a measurement using polycrystalline samples. Here, the NMR/NQR data using crystal No. 1 are shown, but the sample dependence for the spectral shape was negligible. In Fig. 5(a), we observed the broad spectra near the position of zero Knight shift ($H \sim 8$ T) for each temperature. Here, we could not estimate Knight shift owing to the spectral broadening by the quadrupole interaction. At 270 K in the metallic state, the spectrum can be reproduced by a simulation shown by the red curve as a typical powder pattern affected by a quadrupole interaction. We obtained the quadrupole frequency $\nu_Q = 39.8$ MHz and the asymmetry parameter $\eta = 0.2$, which give the resonance frequency of $\nu_{\rm res} = 40.1$ MHz at zero field. As shown in Fig. 5(b), we observed the NQR signal forming a single peak at around 40.0 MHz, which corresponds to $\pm 1/2 \leftrightarrow \pm 3/2$ transition. All the As sites are equivalent in the crystal structure represented by the space group of *Pnma*, which is consistent with these observations. In the NQR spectrum, the spectral width is quite narrow at a high temperature of 320 K, but it is significantly broadened just at $T_{\rm MI1} = 250$ K. In the intermediate temperature range between $T_{\rm MI2}$ and $T_{\rm MI1}$, the NQR spectrum is strongly broadened and almost disappears. The contrastive observation of the NMR signal in the same phase, for which the Zeeman interaction is predominant, excludes a possibility that the fast relaxation weakens the NQR intensity. Therefore, the electric field gradient (EFG) parameters ν_Q and η are suggested to be distributed strongly in this phase. This is in sharp contrast to the ground state below $T_{\rm MI2} = 190$ K,

TABLE II. Structural parameters of RuAs in the metallic and insulating phases. The equivalent isotropic atomic displacement parameter B_{eq} and the occupancy are also shown.

	Site	Wyckoff	x	y	z	B_{eq} (Å^2)	Occup.
293 K	Ru	4c	0.00027	0.25	0.20272	0.59	1
	As	4c	0.19557	0.25	0.56909	0.36	0.988
170 K	Ru1	4e	−0.23004(7)	0.93147(2)	0.26397(5)	0.308(9)	1
	Ru2	4e	0.56805(6)	0.76233(2)	0.56793(5)	0.321(9)	1
	Ru3	4e	0.60492(7)	0.43577(2)	0.60076(6)	0.334(9)	1
	Ru4	4e	0.09791(6)	0.59599(2)	0.59745(5)	0.342(9)	1
	Ru5	4e	−0.27167(7)	0.89775(2)	0.73385(5)	0.336(9)	1
	Ru6	4e	0.07992(6)	0.93010(2)	0.58449(5)	0.278(9)	1
	Ru7	4e	0.25102(6)	0.76444(2)	0.25156(4)	0.298(9)	1
	Ru8	4e	−0.07116(6)	0.72837(2)	0.43422(6)	0.358(9)	1
	Ru9	4e	0.42160(6)	0.59933(2)	0.91880(4)	0.285(9)	1
	As1	4e	−0.28917(8)	0.63657(3)	0.51665(6)	0.268(13)	0.986(3)
	As2	4e	0.63135(8)	0.69241(3)	0.81187(6)	0.231(14)	0.984(3)
	As3	4e	0.05282(8)	0.85291(3)	0.35787(6)	0.222(14)	0.985(3)
	As4	4e	−0.05849(8)	0.80788(3)	0.65457(6)	0.254(14)	0.985(3)
	As5	4e	0.39884(8)	0.52525(3)	0.68557(6)	0.274(14)	0.986(3)
	As6	4e	0.97124(8)	0.47511(3)	0.65011(6)	0.242(14)	0.985(3)
	As7	4e	0.37374(8)	0.85257(3)	0.68016(6)	0.214(14)	0.987(3)
	As8	4e	0.28399(8)	0.68482(3)	0.48169(6)	0.239(13)	0.988(3)
	As9	4e	−0.28604(8)	0.97992(3)	0.51817(6)	0.214(13)	0.988(3)

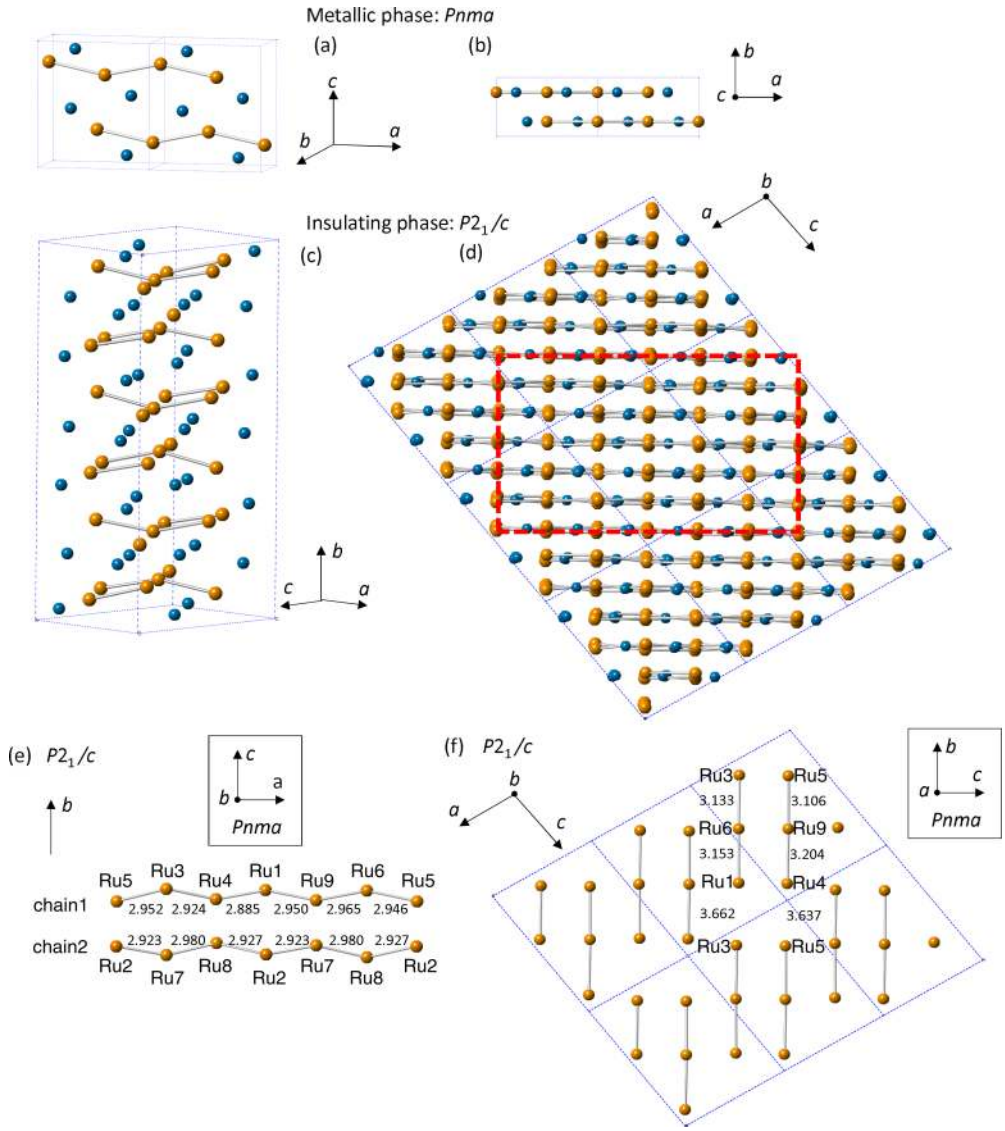

FIG. 4. The crystal structure of RuAs in the metallic phase [(a) and (b): two unit cells are shown.], and in the insulating phase [(c) and (d)]. The blue lines indicate the unit cell of each phase. The orthorhombic $Pnma$ is changed to monoclinic $P2_1/c$ at low temperatures, where new periodicity can be regarded as $3\times3\times3$ for the original unit cell. (e) Zigzag chains of Ru ions. In $Pnma$, all the Ru ions are equivalent, and the zigzag chain is formed by connecting the nearest-neighbor Ru ions, while two types of chains appear in the ground state. The bond lengths of the neighboring Ru ions are shown, but signatures of dimerization or trimerization are not seen. (f) Liner-like chains of the Ru ions, which are a portion of the zigzag ladder along the b axis in the $Pnma$ symmetry. The threefold periodicity of the bond length is clearly observed.

where the sharp signals for the NQR measurement are suddenly recovered, and we observed 8 resonance lines. From this result and the structural analysis, it is clear that the ground state of RuAs is commensurate. On the other hand, the broad and weak NQR intensity in the intermediate phase implies that the charge distribution is incommensurate.

Next, we checked the resonance frequencies at the inequivalent As sites through a first-principles calculation of the EFG using the structural parameters. The calculation method of EFG has been explained elsewhere [18], and it has been used successfully for many systems [19–22]. Here, the nuclear quadrupole moment for the As nucleus, $Q = 314\times10^{-31}$ m^2, is utilized to convert EFG to ν_Q [23]. Table III shows $\nu_Q^{\rm cal}$, $\eta^{\rm cal}$, the resultant resonance frequency $\nu_{\rm res}^{\rm cal}$ estimated from the calculation, and $\nu_{\rm res}^{\rm exp}$ observed experimentally. In the metallic state, the calculated $\nu_Q^{\rm cal}$ is close to the experimental $\nu_Q^{\rm exp} =$ 39.8 MHz estimated from the NMR spectrum, while $\eta^{\rm cal}$ deviates from the experimental $\eta = 0.2$. Since $\nu_{\rm res}$ is not so sensitive to η, $\nu_{\rm res}$ has good consistency between the calculation and the experiment within a small error, which is defined by $(\nu_{\rm res}^{\rm exp} - \nu_{\rm res}^{\rm cal})/\nu_{\rm res}^{\rm exp}$. In the insulating state, $\nu_Q^{\rm cal}$, $\eta^{\rm cal}$, and $\nu_{\rm res}^{\rm cal}$ for all 9 As sites are calculated and shown in ascending order of $\nu_{\rm res}^{\rm cal}$ in the table. The experimental $\nu_{\rm res}^{\rm exp}$ is also listed in ascending order. In the NQR spectrum shown in Fig. 5(b), we observed 8 inequivalent signals; therefore, 1 site is missing. The intensity analysis in the wide frequency range is difficult to keep accurate, but the signal just below 50 MHz has the largest intensity (area) and the broadest width among the 8 signals, indicating that 2 peaks are accidentally overlapped in the signal. This interpretation is strongly supported by the

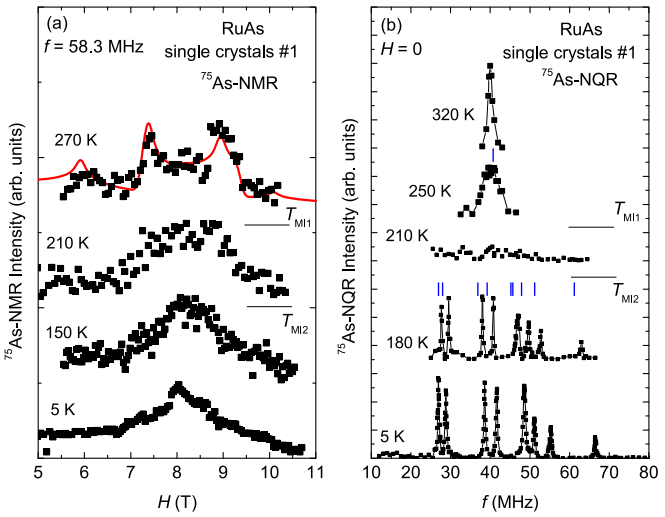

FIG. 5. (a) Field-swept NMR spectrum for RuAs measured at around 8 T. (b) NQR spectrum for RuAs measured at zero field. In the metallic state above T_{MI1}, the NMR spectrum obtained using many pieces of single crystals shows a typical powder pattern by assuming the unique As site, as shown by the red curve. This is consistent with the NQR spectrum observed at around 40.0 MHz. Below T_{MI1}, the broadened NMR spectrum and the suppression of the NQR intensity indicate the strong distribution of ν_Q and η. In the ground state below T_{MI2}, several peaks are observed at the NQR measurement, indicative of the formation of the superlattice. The blue lines indicate the resonance frequencies calculated using the structural parameters at 293 K and 170 K.

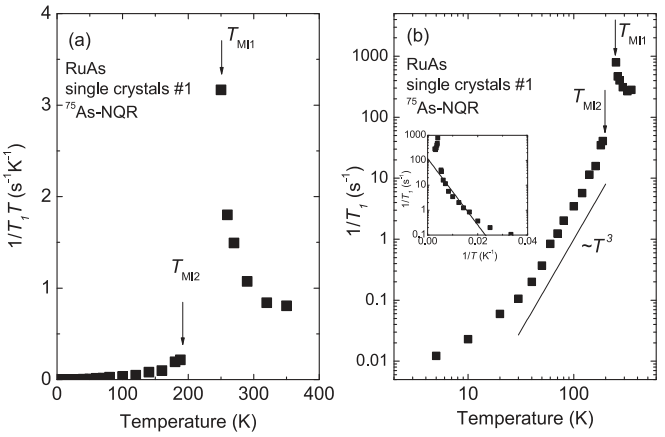

FIG. 6. Temperature dependence of (a) $1/T_1T$ and (b) $1/T_1$ for RuAs. RuAs undergoes the insulating state accompanied by a strong development of some fluctuations. The T^3 behavior below T_{MI2} indicates that the energy gap of RuAs is anisotropic.

calculation, in which the As1 and As8 sites have almost the same resonance frequencies, which are slightly smaller than the subjected resonance frequency. In this context, the $\nu_{\mathrm{res}}^{\mathrm{exp}}$ values for all the As sites show an almost regular error of about $+2.4 \sim 5.1$ % for the calculation. The resultant $\nu_{\mathrm{res}}^{\mathrm{cal}}$ are shown by the blue lines in Fig. 5(b) for each phase. The present calculation reproduces excellently the EFG at the As sites, ensuring the high validity of the obtained structural parameters as well as the reliability of the calculation. Simultaneously, this result reveals that the ground state of RuAs is nonmagnetic, because the spectral splitting by the internal field can be ignored.

TABLE III. Calculated and experimental EFG parameters of RuAs in the metallic and insulating phases.

Metallic phase					
		293 K		290 K	
Site	ν_Q^{cal} (MHz)	η^{cal}	$\nu_{\mathrm{res}}^{\mathrm{cal}}$ (MHz)	$\nu_{\mathrm{res}}^{\mathrm{exp}}$ (MHz)	Error (%)
As	36.7	0.833	40.7	40.0	−1.8
Insulating phase					
		170 K		180 K	
Site	ν_Q^{cal} (MHz)	η^{cal}	$\nu_{\mathrm{res}}^{\mathrm{cal}}$ (MHz)	$\nu_{\mathrm{res}}^{\mathrm{exp}}$ (MHz)	Error (%)
As6	25.68	0.551	26.95	27.6	+2.4
As2	25.35	0.810	27.99	29.5	+5.1
As7	35.39	0.508	36.89	38.0	+2.9
As9	37.65	0.508	39.24	40.9	+4.1
As1	40.70	0.837	45.20	47.0	+3.8
As8	43.47	0.562	45.70	47.0	+2.8
As3	47.13	0.317	47.91	49.7	+3.6
As4	48.76	0.554	51.19	52.7	+2.9
As5	54.71	0.869	61.22	62.9	+2.7

Figure 6(a) shows the temperature dependencies of $1/T_1T$ for the single crystal of RuAs. T_1 was measured at the peak of ∼49 MHz in the insulating state, and at the single peak at ∼40 MHz in the metallic state. Unfortunately, we could not measure T_1 in the intermediate region between T_{MI1} and T_{MI2} owing to the weak intensity. The $1/T_1T$ shows a strong divergence toward T_{MI1} and obvious suppression below T_{MI2}. The divergence shows that a symmetry lowering by the metal-insulator transition is accompanied by strong critical fluctuations. Since the As nuclear spin is $I = 3/2$, both magnetic and electric relaxations are possible for the origin of the divergence of $1/T_1$. The absence of Curie-Weiss-like behavior in magnetic susceptibility suggests that the magnetic correlation of $\vec{q} = 0$ is weak in this system, but the concerned wave vector is probably finite, because the superlattice of $3\times3\times3$ is formed at the low temperatures. $1/T_1T$ corresponds to a $\vec{q}$-summed dynamical susceptibility. Therefore, the presence of magnetic correlations cannot be excluded experimentally at present. Figure 6(b) displays the temperature dependence of $1/T_1$ for RuAs. $1/T_1$ in RuAs follows T^3 behavior below T_{MI2} in contrast to a conventional exponential behavior. One possibility is that the relaxation at low temperatures is extrinsically dominated by a small number of magnetic impurities. We cannot exclude this possibility because the Curie tail appears in the susceptibility at low temperatures. Another possibility is intrinsically that the density of states (DOS) near the Fermi energy, E_F, has a linear energy dependence, that is, $D(E') \sim |E'|$, where $E' = E - E_F$, unlike a simple full gap. The thermal excitation in this energy dependence gives T^3 dependence in $1/T_1$. If this is the case, the band structure near E_F is expected to be like a semimetal. We cannot judge which is correct, but an estimation of the energy gap was tried for a comparison

by the same manner as that attempted for RuP [7]. Using $1/T_1 \sim \exp(-E_g/k_BT)$ for the experimental data between T_{MI2} and 50 K, as shown in the inset of Fig. 6(b), we obtained $E_g = 308$ K $\pm$ 30 K, which is comparable to 340 K estimated from the resistivity in the same temperature range. The energy gap of RuAs is several times smaller than 1250 K for RuP [7], which is qualitatively consistent with a difference in the resistivity between the two compounds [6].

D. Electronic structure calculation

Figures 7(a) and 7(b) show the calculated energy dispersion and the DOS for the metallic phase in the *Pnma* space group, and the Fermi surfaces are drawn in Fig. 8. In the energy dispersion, the flat bands near E_F are seen along the *T*-*R*, *S*-*R*, and partially *Y*-*S* axes, and they construct the peak structure in the DOS near E_F. This feature is consistent with the previous calculation [8]. The spin-orbit coupling is taken into account in the present calculation, the DOS is slightly modified, and the peak feature near E_F becomes more remarkable. The band splitting by the spin-orbit coupling can be seen along the specific axes, such as *S*-*X*, *Z*-*T*, and *Y*-*T*, where only twofold spin degeneracy remains. However, the fourfold degeneracy is completely maintained, for example, along the *Y*-*S*, *T*-*R*, and *S*-*R* axes, which are on the Brillouin zone boundary, as indicated by red lines in Fig. 7(a), because it is protected by the nonsymmorphicity of the *Pnma* space group [24]. This feature will be a common point to contribute an electronic state of systems in the nonsymmorphic *Pnma* space group; for instance, it can be a key ingredient to interpret a magnetoresistance of the isostructural CrAs [24]. This protection yields the almost degenerate Fermi surfaces near the Brillouin zone boundary in the metallic phase of RuAs. The platelike Fermi surfaces with a hollow in the middle are seen in 63 and 64 electron bands, and they partially degenerate because of the protected degeneracy along the *Y*-*S*, *T*-*R*, and *S*-*R* axes. Interestingly, the flat bands near E_F exist along the axes with the fourfold degeneracy protected by the crystal symmetry. This certainly produces the peak structure in the DOS and makes this phase unstable at low temperatures; therefore, the lifting of this degeneracy by a symmetry lowering from the nonsymmorphic *Pnma* is a key ingredient of the metal-insulator transition.

We test a band calculation for the ground state in the $P2_1/c$ space group, and the energy dispersion in the vicinity of E_F and the DOS are shown in Fig. 9. Here, the Brillouin zone is that of the monoclinic structure. We can confirm a disappearance of the degenerate flat bands, but the present calculation did not produce a clear energy gap, which is relatively small as it is estimated to be $E_g = 340$ K ~ 0.03 eV from the resistivity. The result shows a semimetallic band dispersion as an important feature; two electron bands and two hole bands cross E_F, and a switching of the electron bands and the hole bands does not occur in the momentum space. As a result, a valley of DOS near E_F approximates a gaplike feature, as shown in the inset of Fig. 9(b). The DOS at E_F of ~5600 states/eV is significantly reduced from ~12000 states/eV for the 9 unit cells in the metallic phase. However, the absence of a clear gap in the calculation indicates the presence of some lacking factor to reproduce the electronic state of the ground state completely. Generally, the LDA calculation tends to

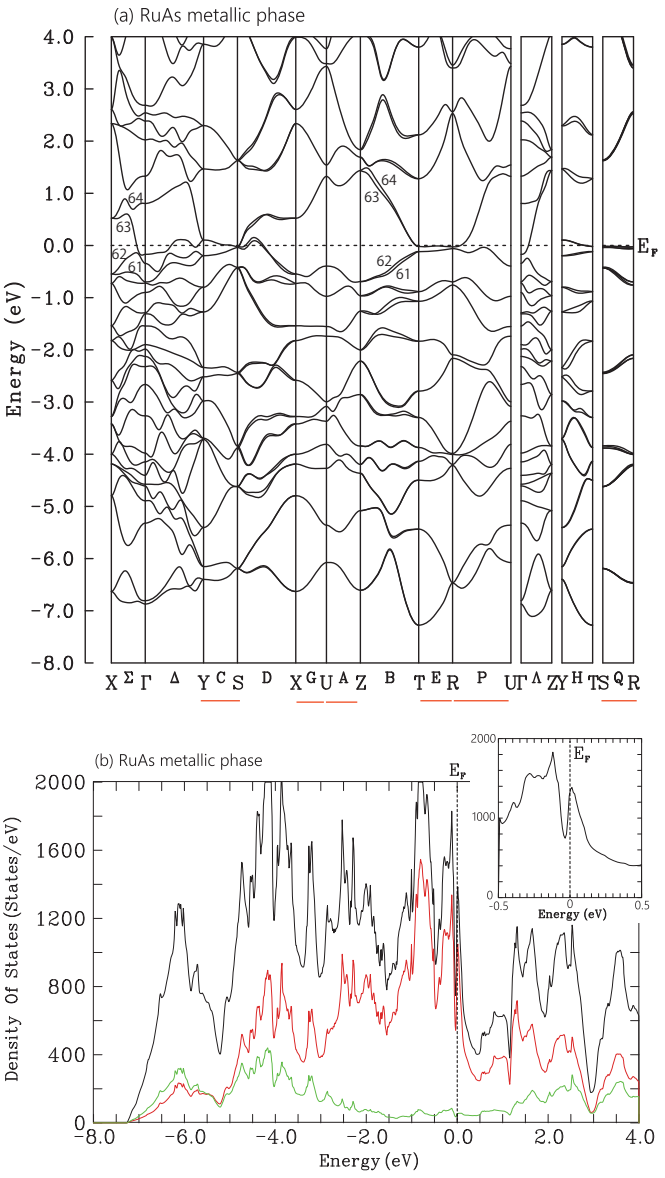

FIG. 7. The calculated energy dispersion and the DOS of RuAs in the metallic phase in the orthorhombic *Pnma* space group. The fourfold degeneration is realized along axes shown by red lines in the Brillouin zone boundary even though the spin-orbit coupling is considered, because of the protection by the nonsymmorphic symmetry. Two hole bands and two electron bands denoted by 61–64 cross the Fermi level. The flat bands near E_F are seen along the degenerated *Y*-*S*, *T*-*R*, and *S*-*R* axes, producing the large DOS at E_F. In the lower panel, the black curve indicates the total DOS integrated in the whole k space. The red and green curves indicate the partial DOS originating from the Ru-4d and As-4p orbitals, respectively.

underestimate the energy gaps of semiconductors or insulators [25,26]. This is interpreted as inaccuracy in the approximation itself; therefore, it may be difficult to reproduce the small energy gap of ~0.03 eV in the LDA framework. In other words, inadequate consideration of the Coulomb interaction causes the underestimation of the gap. The energy gap in principle may open by increasing the Coulomb interaction numerically in the semimetallic electronic state, although the energy shift of

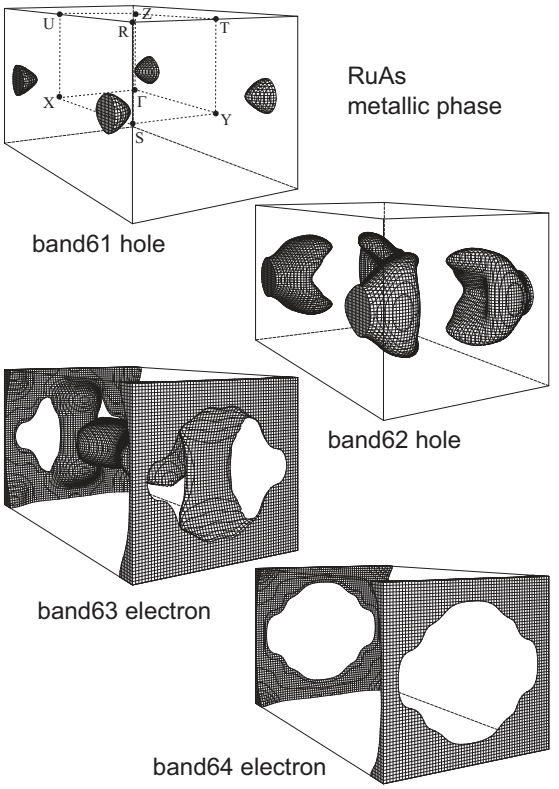

FIG. 8. The Fermi surfaces of RuAs in the metallic phase in the *Pnma* space group. The 63 and 64 electron sheets are almost degenerated and low-dimensional.

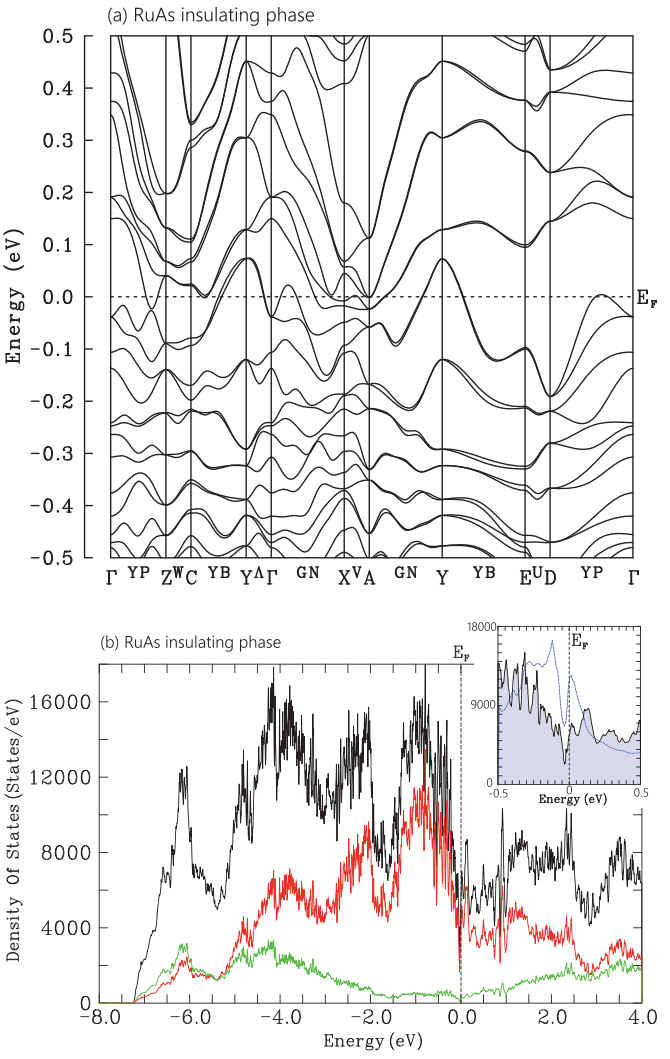

FIG. 9. The calculated energy dispersion in the vicinity of E_F and the DOS of RuAs in the insulating phase in the monoclinic $P2_1/c$ space group. A gaplike feature is likely to appear in the DOS near E_F. In the lower panel, the black curve indicates the total DOS integrated in the whole k space. The red and green curves indicate the partial DOS originating from the Ru-4d and As-4p orbitals, respectively. In the inset, the solid line with the hatched region indicates the total DOS for the insulating state, while the dotted line shows the metallic state. Here, the DOS of the metallic phase is multiplied by 9 to adjust the difference in the size of the unit cell.

approximately 0.1 eV between the electron and hole bands is required in this case. In any case, the development of the gaplike feature accompanied by the semimetallic band structure suggests that the lifting of the degeneracy through the formation of the superlattice promotes producing the insulating state. In this sense, the transition is caused by a band Jahn-Teller effect.

Another important point is why the superlattice of $3\times3\times3$ is necessary at low temperatures, because the superlattice formation is not essential to lift the degeneracy protected by nonsymmorphic symmetry. RuAs itself is a compensated metal in the *Pnma* space group, and it can be insulating with maintaining the size of the unit cell. For example, the simple dimerization along the zigzag chain (along the a axis in *Pnma*), which does not change the size of the unit cell, can lift this degeneracy, but this is not realized. To check a relationship between the structural modulation and the electronic state, we evaluated the d-electron number of each Ru site in the insulating state, which was obtained in the band calculation, and they are shown in Table IV. The average number of d electrons at all the Ru sites is 5.299, which corresponds to $Ru^{2.701+}$. The differences from the average number at each Ru site are also listed in the table. The d-electron numbers at the Ru6, Ru7, and Ru9 sites are obviously fewer than those of other sites. An arrangement of these Ru ions in the crystal structure is shown in Fig. 10, where the Ru6, Ru7, and Ru9 sites are drawn by green spheres and the As sites are eliminated. The upper right structure is the ac plane in the $P2_1/c$ space group, which is equivalent to that in Fig. 4(d), and the lower figure shows each layer normal to the ac plane. These layers are the bc plane in the original *Pnma* space group, and it consists of the zigzag ladders. As shown in the upper left structure, the zigzag ladder was constructed by the equivalent Ru sites in the metallic phase, and it deforms in the insulating state. The shorter Ru-Ru bondings, whose length is less than 3.21 Å, are shown in the lower figure. As already shown in Fig. 4, some bondings obviously extend, making a clear threefold periodicity along the original b axis. The Ru6, Ru7, and Ru9 sites possess 4 shorter bondings in the layer, while other sites have 3 shorter bondings. This difference is likely to induce the distribution of the d-electron numbers. Interestingly, the Ru6, Ru7, and Ru9 sites align in a straight line

TABLE IV. Calculated d-electron numbers at each Ru site in the insulating phase.

Insulating phase		
Site	d-electron number	Difference from the average (%)
Ru1	5.301	+0.038
Ru2	5.305	+0.113
Ru3	5.303	+0.075
Ru4	5.310	+0.208
Ru5	5.301	+0.038
Ru6	5.291	−0.151
Ru7	5.290	−0.170
Ru8	5.304	+0.094
Ru9	5.286	−0.245

in this layer, indicative of the formation of a stripe-type charge modulation. Reflecting the original zigzag chain along the a axis in the $Pnma$ space group, which is perpendicular to these layers, the direction of the stripe changes alternatively layer by layer. This apparent coupling of the structural and electronic modulations suggests the formation of a commensurate CDW in the ground state of RuAs. It is conjectured that the $3\times3\times3$ superlattice is required to produce this structural and electronic modulation. Numerical studies are required to elucidate why this modulation is the most stable at low temperatures. In this context, a contribution of the nesting of the Fermi surfaces is also a matter of concern. The nesting property with the corresponding wave vector will be checked by a numerical analysis in the future.

IV. SUMMARY

In summary, several experiments have been performed for single crystals of RuAs obtained successfully using the Bi-flux method. These show clear successive metal-insulator transitions at $T_{MI1} \sim 255$ K and $T_{MI2} \sim 195$ K like the polycrystalline sample. This enables us to escape from an awkward problem on the sharp difference between the poly- and single crystals of RuP. The x-ray structural analysis and the NQR spectrum for RuAs demonstrate the nonmagnetic superlattice of $3\times3\times3$ is formed in the ground state, while the detailed structure and electronic state in the intermediate phase are unclear yet. Although the decided superlattice structure of the ground state is complicated, the validity is guaranteed

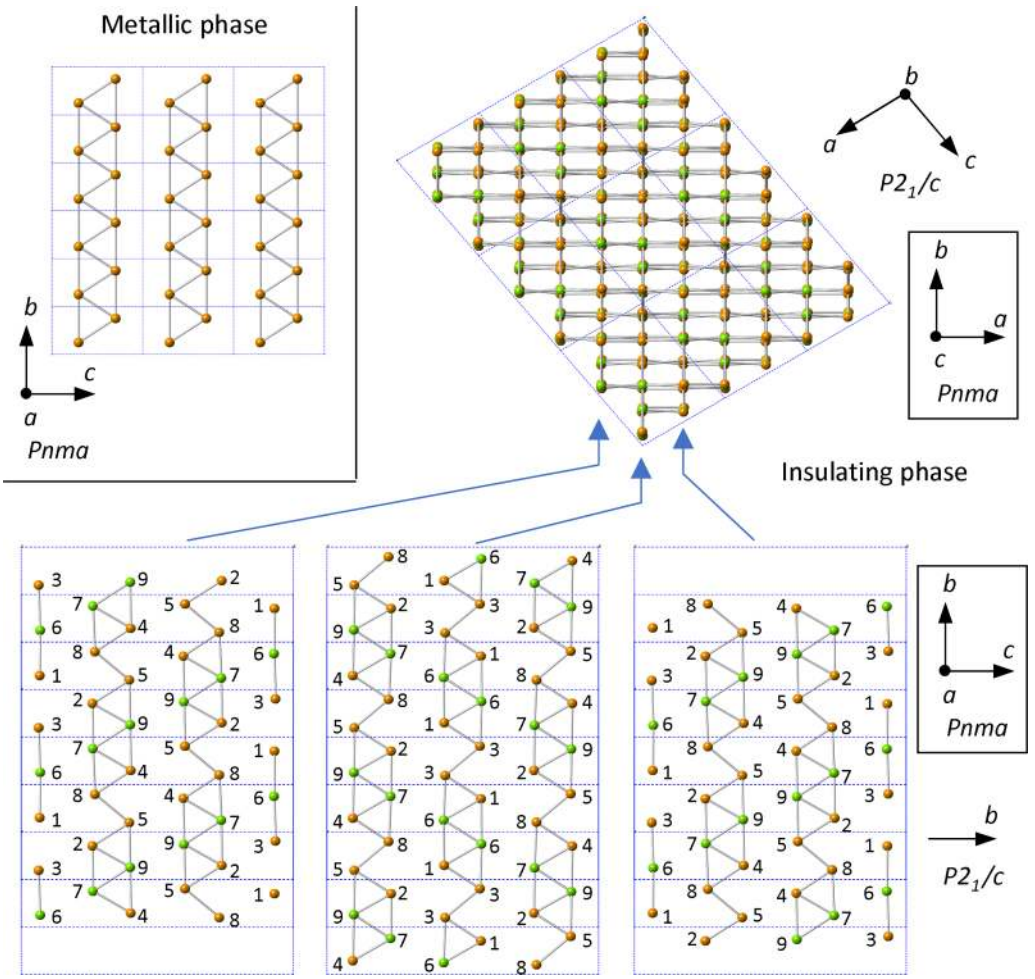

FIG. 10. The arrangement of the Ru ions in the metallic state (upper left) and the insulating state (upper right and lower). In the metallic phase, the Ru ions form the zigzag ladder along the b direction. In a lower structure, the number indicates each Ru site. The Ru6, Ru7, and Ru9 sites, where the calculated electron numbers are fewer, are shown by green spheres. In the bc plane of the original $Pnma$ structure, a linear alignment of those sites is realized. In the lower structure, the shorter Ru-Ru bonding of less than 3.21 Å is drawn.

strongly through the excellent agreement of the quadrupole frequencies between the experiment and the calculation. The revealed crystal structure does not show a clear indication of dimerization of the Ru ions, and an odd number of Ru sites in the unit cell excludes the possibility of a spin-singlet formation. The structural modulation and its clear coupling with the calculated d-electron number suggests the formation of a stripe-type CDW, where the direction of the stripe alternates layer by layer. A direct observation of this electronic modulation is an important issue, and a verification of the orbital state at each Ru site is also an interesting subject. RuAs is not a simple low-dimensional material but possesses the Fermi surface instability caused by a nonsymmorphicity of the *Pnma* space group, resulting in the transition to the insulating state with the characteristic structural and electronic modulation.

ACKNOWLEDGMENTS

The authors thank Y. Kuramoto, S. Kimura, D. Hirai, A. Koda, and H. Ikeda for helpful discussions. This work has been supported in part by Grants-in-Aid for Scientific Research (No. 15H03689, No. 15H05745, No. 15H05882, and No. 15H05885) from the Ministry of Education, Culture, Sports, Science, and Technology (MEXT) of Japan.

[1] R. E. Peierls, Ann. Phys. Leipzig **396**, 121 (1930).
[2] E. Pytte, Phys. Rev. B **10**, 4637 (1974).
[3] D. I. Khomskii and T. Mizokawa, Phys. Rev. Lett. **94**, 156402 (2005).
[4] S. V. Streltsov and D. I. Khomskii, Phys. Rev. B **89**, 161112(R) (2014).
[5] H. Harima, J. Phys. Soc. Jpn. **77**, 114 (2008).
[6] D. Hirai, T. Takayama, D. Hashizume, and H. Takagi, Phys. Rev. B **85**, 140509(R) (2012).
[7] S. Li, Y. Kobayashi, M. Itoh, D. Hirai, and H. Takagi, Phys. Rev. B **95**, 155137 (2017).
[8] H. Goto, T. Toriyama, T. Konishi, and Y. Ohta, Phys. Proc. **75**, 91 (2015).
[9] K. Sato, D. Ootsuki, Y. Wakisaka, N. L. Saini, T. Mizokawa, M. Arita, H. Anzai, H. Namatame, M. Taniguchi, D. Hirai, and H. Takagi, arXiv:1205.2669.
[10] R. Y. Chen, Y. G. Shi, P. Zheng, L. Wang, T. Dong, and N. L. Wang, Phys. Rev. B **91**, 125101 (2015).
[11] G.-Z. Fan, R.-Y. Chen, N.-L. Wang, and J.-L. Luo, Chin. Phys. Lett. **32**, 077203 (2015).
[12] S. Rundqvist, Acta Chem. Scand. **16**, 287 (1962).
[13] T. C. Kobayashi, H. Hidaka, H. Kotegawa, K. Fujiwara, and M. I. Eremets, Rev. Sci. Instrum. **78**, 023909 (2007).
[14] K. Murata, K. Yokogawa, H. Yoshino, S. Klotz, P. Munsch, A. Irizawa, M. Nishiyama, K. Iizuka, T. Nanba, T. Okada, Y. Shiraga, and S. Aoyama, Rev. Sci. Instrum. **79**, 085101 (2008).
[15] G. M. Sheldrick, Acta Crystallogr., Sect. A **64**, 112 (2008).
[16] A. L. Spek, J. Appl. Crystallogr. **36**, 7 (2003).
[17] B. Saparov, J. E. Mitchell, and A. S. Sefat, Supercond. Sci. Technol. **25**, 084016 (2012).
[18] P. Blaha, K. Schwarz, and P. Herzig, Phys. Rev. Lett. **54**, 1192 (1985).
[19] P. Blaha, K. Schwarz, W. Faber, and J. Luitz, Hyperfine Interact. **126**, 389 (2000).
[20] K. Schwarz, C. Ambrosch-Draxl, and P. Blaha, Phys. Rev. B **42**, 2051 (1990).
[21] H. Harima, Physica B **378–380**, 246 (2006).
[22] Ján Rusz, P. M. Oppeneer, N. J. Curro, R. R. Urbano, B.-L. Young, S. Lebégue, P. G. Pagliuso, L. D. Pham, E. D. Bauer, J. L. Sarrao, and Z. Fisk, Phys. Rev. B **77**, 245124 (2008).
[23] P. Pyykkö, Mol. Phys. **106**, 1965 (2008); P. Pyykkó, *ibid.* **99**, 1617 (2001).
[24] Q. Niu, W. C. Yu, K. Y. Yip, Z. L. Lim, H. Kotegawa, E. Matsuoka, H. Sugawara, H. Tou, Y. Yanase, and S. K. Goh, Nat. Commun. **8**, 15358 (2017).
[25] N. W. Ashcroft, N. D. Mermin, and D. Wei, *Solid State Physics*, rev. ed. (Singapore Cengage Learning, 2016), p. 314.
[26] X. Zheng, A. J. Cohen, P. Mori-Sánchez, X. Hu, and W. Yang, Phys. Rev. Lett. **107**, 026403 (2011).